# Journal Pre-proof

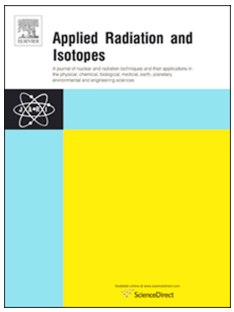


Effects on the accelerating electron bunches due to the presence of sulfur hexafluoride or air in the linac waveguide

A. Gayol, R. Figueroa, J. Guarda, J. Leiva, F. Leyton, F. Malano, M. Valente

PII: S0969-8043(23)00508-0

DOI: https://doi.org/10.1016/j.apradiso.2023.111155

Reference: ARI 111155

To appear in: *Applied Radiation and Isotopes*

Received Date: 6 February 2023

Revised Date: 8 November 2023

Accepted Date: 19 December 2023

Please cite this article as: Gayol, A., Figueroa, R., Guarda, J., Leiva, J., Leyton, F., Malano, F., Valente, M., Effects on the accelerating electron bunches due to the presence of sulfur hexafluoride or air in the linac waveguide, *Applied Radiation and Isotopes* (2024), doi: https://doi.org/10.1016/j.apradiso.2023.111155.

# Effects on the accelerating electron bunches due to the presence of sulfur hexafluoride or air in the linac waveguide

A. Gayol[1], R. Figueroa[2,3], J. Guarda[2], J. Leiva[2], F. Leyton[2], F. Malano[2,3], & M. Valente[1,2,3]

[1] Instituto de Física Enrique Gaviola, CONICET & Laboratorio de Investigaciones e Instrumentación en Física Aplicada a la Medicina e Imágenes por Rayos X - LIIFAMIR[x], FAMAF, Universidad Nacional de Córdoba, Córdoba, 5000, Argentina
[2] Centro de Física e Ingeniería en Salud CFIS, Universidad de la Frontera, Temuco, 4780000, Chile
[3] Departamento de Ciencias Físicas, Universidad de la Frontera, Temuco, 4780000, Chile

## Abstract

Sulphur hexafluoride gas (SF6) is used as a dielectric insulator in the acceleration process of certain medical linear accelerator waveguides. Nevertheless, some innovative development and investigation cases require intervention in the linear accelerator or, specifically, on the waveguide, which could affect the sealing of the device. In this regard, vacuum sealing systems can be compromised, affecting the properties of the radiation beams produced. The presence of sulfur hexafluoride or air inside the VARIAN 6/100 waveguide was investigated under different pressure conditions and non-uniform electric fields, adapting Monte Carlo simulation techniques for modeling radiation transport coupled with electric fields. Obtained results indicated the suitability of the proposed approach, while comparisons with theoretical approaches and experimental evidence supported the model's consistency.

*Key words:* *Linac VARIAN 6/100; Waveguide; Sulfur hexafluoride; Electric field.*



## Introduction

Clinical linear accelerators (linacs) are devices that accelerate charged particles, such as electrons, by means of high frequency electromagnetic waves to high energies (Khan, 2003). Electrons are injected in the system and then accelerated following straight trajectories inside a specific structure called *accelerating waveguide*, which they travel several times under a potential difference (Podgorsak, 2005).

A cavity made of a conducting material, such as copper, represents the waveguide. Both rectangular and circular cross sections are used to confine microwaves by reflection from their walls (Karzmark & Morton, 1989). Particularly and of special interest for this work, medical linac accelerating waveguides are basically constituted by a cylindrical copper tube containing in its interior a periodic array of conducting disks with axial holes, of variable aperture and size, called dynodes (Podgorsak, 2006). These disks form the basic structure of the accelerating waveguide, dividing it into a series of cylindrical holes that operate as the resonant cavities of the system. As electrons enter the accelerating waveguide region with an initial energy of the order of tenths of keV, they interact with the electric field of the traveling wave increasing their

kinetic energy due to the sinusoidal character of the field (Karzmark & Morton, 1989; Whittum, 1998).

When a charged particle is in the presence of an electric field, according to the Lorentz formulation, it experiences a force equal to the product between its charge and the field (Jackson, 1999). Mechanical effects come from the work done by the electric force on the charge distribution. According to the Newton's second law, independently on the path taken between the endpoints (Zangwill, 2012), electrons inside the waveguide will be accelerated moving forward the central axis as a consequence of the work made by the electric field on them.

The high-power radio frequency (RF) for accelerating electrons is transported to the waveguide, so sulfur hexafluoride gas (SF6) is used by the VARIAN 6/100 waveguide as dielectric insulator in the first acceleration stage. In a standard linac the electron acceleration waveguide needs to be in a ultra-high vacuum to avoid collisions between the electron bunches being accelerated with scattering centers, like atoms or molecules that might be present along the path. The waveguide carrying the RF from the magnetron to the acceleration waveguide behaves as any microwave waveguide, thus the propagation of the RF energy in the hollow cavity is based on conductive walls acting as distributed inductors and the space between walls acting as distributed capacitors. Thus, the waveguide is pressurized with dielectric gasses, like the $SF_6$, which reduces the possibility of electrical breakdown and thus increases their power-handling capacity (Karzmark & Morton, 1989). Due to its high electronegativity, negative ions are established by attachment of electrons with neutral molecules, and consequently free charge carriers are dissipated (Goller, 2008). In this context, the specific physical-chemical and electrical characteristics of the SF6 have enabled its successful application as a dielectric material (Glushkov et. al., 2014; Pedersen, 1989). Therefore, this gas is typically employed to perform high-voltage electrical cut-off and insulation functions, being the pressure one of the most important parameters to consider, in accordance with the European standard EN 62271-1 (European Standards, 2021). Since interactions between matter and ionizing radiation may generate a loss of energy, for guaranteeing an effective energy transfer from the electromagnetic wave to the electron beam, it is mandatory that these types of devices are vacuum sealed (Wangler, 1989).

There are some cases where interventions on the waveguide for development and investigation purposes are required that could impair the sealing of the device. For instance, Yaqub et.al. (2021) have designed a linac that offers the possibility of replacing the electron gun, RF window and X-ray target. Wisnivesky et. al. (1997) design modifications to increase the energy of a linac, also using SF6 as an insulator in the new version of the device. There are even cases where, due to the age and the constant use of the equipment, a gas leak (air or SF6) could occur and compromise the vacuum system. Particularly, the CONVERAY project at the Center for Physics and Engineering for Health (CFIS) - Universidad de la Frontera - Chile, aims to develop a device capable of concentrating the linac photon beam for treatment (Figueroa & Valente, 2015; Figueroa & Valente, US20140112451A1; Figueroa et al., 2016). As part of this project, a 6 MV VARIAN linac waveguide was modified, replacing the original Tungsten target with a thin Beryllium or Titanium window.

In all these cases where part of the waveguide is manipulated, a proper sealing is essential to guarantee accelerator operation, since the vacuum system plays a significant role,

as mentioned for Wroe et.al. (2019) and Reece et.al. (2001) for example. However, access to vacuum pumps or equipment to achieve adequate vacuum levels is difficult, very expensive and time consuming. Even in cases where gas leaks are suspected in the waveguide, it is often decided to replace the entire waveguide, which is expensive as well. In this context, having a simpler and more affordable tool to study the spectral degradation of accelerated electrons as a function of gas type and pressure, is extremely useful in determining the level of vacuum required for the particular application or use to which the waveguide will be subjected. Therefore, the aim of the present work arises from the need of study and characterization of situations in which the linac design has been modified, inducing possible vacuum leaks, presence of matter in the accelerating waveguide or probability of extensive degassing for example.

For this purpose dedicated Monte Carlo (MC) simulations have been performed to point out the effects due to the presence of air or SF6 inside a 6 MV VARIAN linac accelerating waveguide. Moreover, effects on primary and secondary particle fluence have been carefully characterized for both gasses considering different pressure conditions. Several authors have conducted radiation transport numerical studies to complement measurements in biomedical applications (Figueroa et. al., 2015; Valente et. al., 2007) as well as focusing on linacs' operation characteristics (Gündem & Dirican, 2021; Rodriguez Castillo et.al., 2020; Mohammed et. al., 2018). For instance, Aubin et. al. (Aubin et.al., 2010) reported an interesting work modeling a 6 MV linac accelerator including the electron gun and the RF field, solving by the finite elements method and separating the accelerating waveguide in short sections. On the other hand, Yaqub et.al. (2021) have taken special interest in the design of a vacuum system for a commercial 6 MeV linac, remarking the importance of a proper sealing for guaranteeing the functioning of the accelerator. Nevertheless, none of those studies include the possible presence of gas inside the waveguide while considering the effects of spatially variable, *i.e.* non-uniform, electric fields.



## Materials and Methods

The proposed approach to study the effects due to the presence of gas inside the accelerating waveguide is based on MC simulations, which have been performed by dedicated adaptations of the FLUKA main code. Besides, basic thermodynamics has been used to account for different gas pressure levels in the waveguide. Finally, dedicated data processing allowed to obtain the longitudinal fluence both for primary and secondary particles.

### Monte Carlo simulation code FLUKA

Monte Carlo simulation methodologies involve a group of computational algorithms, which by means of random variables generation process, estimate numerically the value of unknown parameters (Sickafus et.al., 2007). In this sense, the MC technique offers solutions for macroscopic systems by means of the simulation of the microscopic interactions of its components (Bielajew & Boulevard, 2000). Thereby, MC techniques have proved to be particularly suitable for solving numerically definite integrals, allowing its application for

modeling the radiation transport under the Boltzmann formalism (Aubin et.al., 2015; Berger, 1963). Within the medical physics framework, MC simulations are commonly used as a tool for solving a wide variety of problems, ranging from output spectra of therapy units to the characterization of dosimetry systems, for instance.

The FLUKA MC main code (Battistoni et.al., 2016; Bohlen et.al., 2014) is integrated with the python-based FLAIR graphical interface that assists the user to create and edit input files, as well as to visualize simulation geometry and outputs. Particularly, this code has shown great capacity and precision for modeling the radiation transport in different materials for medical physics purposes (Malano et al., 2019; Kozłowska et al., 2019; Vedelago et al., 2018), considering the presence of electromagnetic (EM) fields through user defined subroutines. FLUKA has been thoroughly benchmarked against experimental and theoretical data both from research and clinical applications in medical physics [Battistoni et al., 2011, Gayol et al., 2022]. Moreover, the recently extended FLUKA capabilities make it possible to carry out the present study involving electric fields' effects on charged particles' transport mechanisms.

The current distribution of the FLUKA code, property of the Italian National Nuclear Institute (INFN) and the European Organization for Nuclear Research (CERN), implements Runge-Kutta methods for describing with a high degree of precision the coupling between charged particles and electric fields, in vacuum and low-density medium, like gasses (Ferrari et.al., 2021). For this purpose, Kugland step theory (Ehret, 2016) has been employed, as depicted in Figure 1. The deviation angle of the charged particle (α) can be assessed within the Kugland sketch, which attains good performance for small deviations.

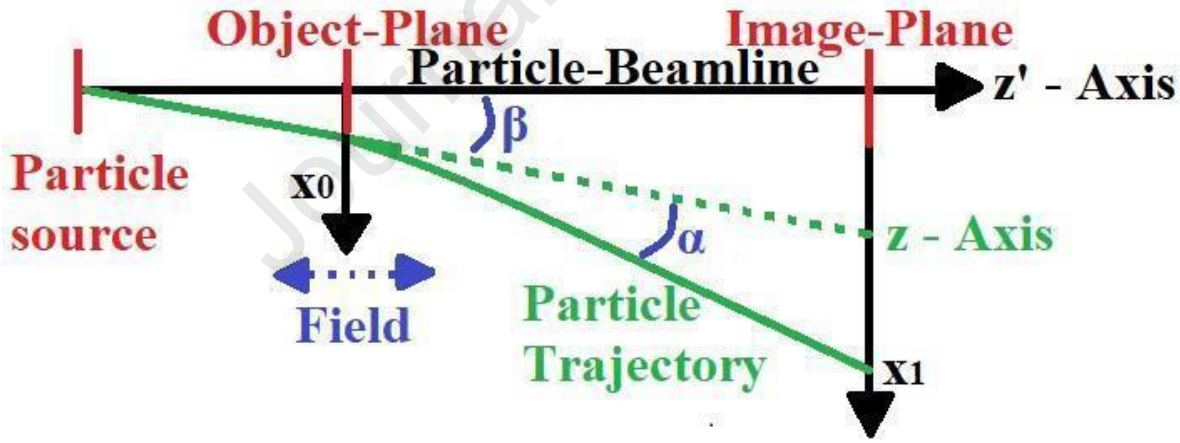


Figure 1: Kugland steps' basic geometrical relations. Assumptions: the field zone of influence ("Field") should be significantly smaller than the distance in between the field source and the particle source plane (left red line) and the distance between image and object planes (central and right red lines) are used to calculate the corresponding magnifications.

Charged particles' transport in the FLUKA code is affected by the presence of EM fields by means of tracking modifications according to the EM interactions. Specifically, the tracking is accomplished by implementing a Runge-Kutta-Gill 4th order algorithm for the combined electric and magnetic (if any) fields. Thus, main effects like changes of the projectile energy due to the interaction with the electric field are accounted for. Nevertheless, it should be pointed

out that some approximations are introduced to model the particle transport in the presence of EM fields, the “true trajectory” is decomposed in small straight-line steps; for instance.

## Simulation set up

The FLUKA MC code has been adapted and implemented with the aim of studying the influence, on primary and secondary particles inside the VARIAN 6/100 linac waveguide, of the electric field for different pressures and for both air and SF6. Figure 2 shows the MC model along with the actual waveguide 30 cm long, approximately.

Briefly, the waveguide interior has been modeled as a ~30 cm cylindrical cavity, 1 cm diameter with a copper surrounding structure for the solid piece of the guide. The dynodes’ array has been designed as a series of spherical/cylindrical cavities of 4 cm long, 1 cm apart each one (Baillie, 2016). In addition, as depicted in Figure 2, cavities on the upper and lower part of the waveguide have also been included according to technical details provided elsewhere (VARIAN, 1981; Baillie, 2016).

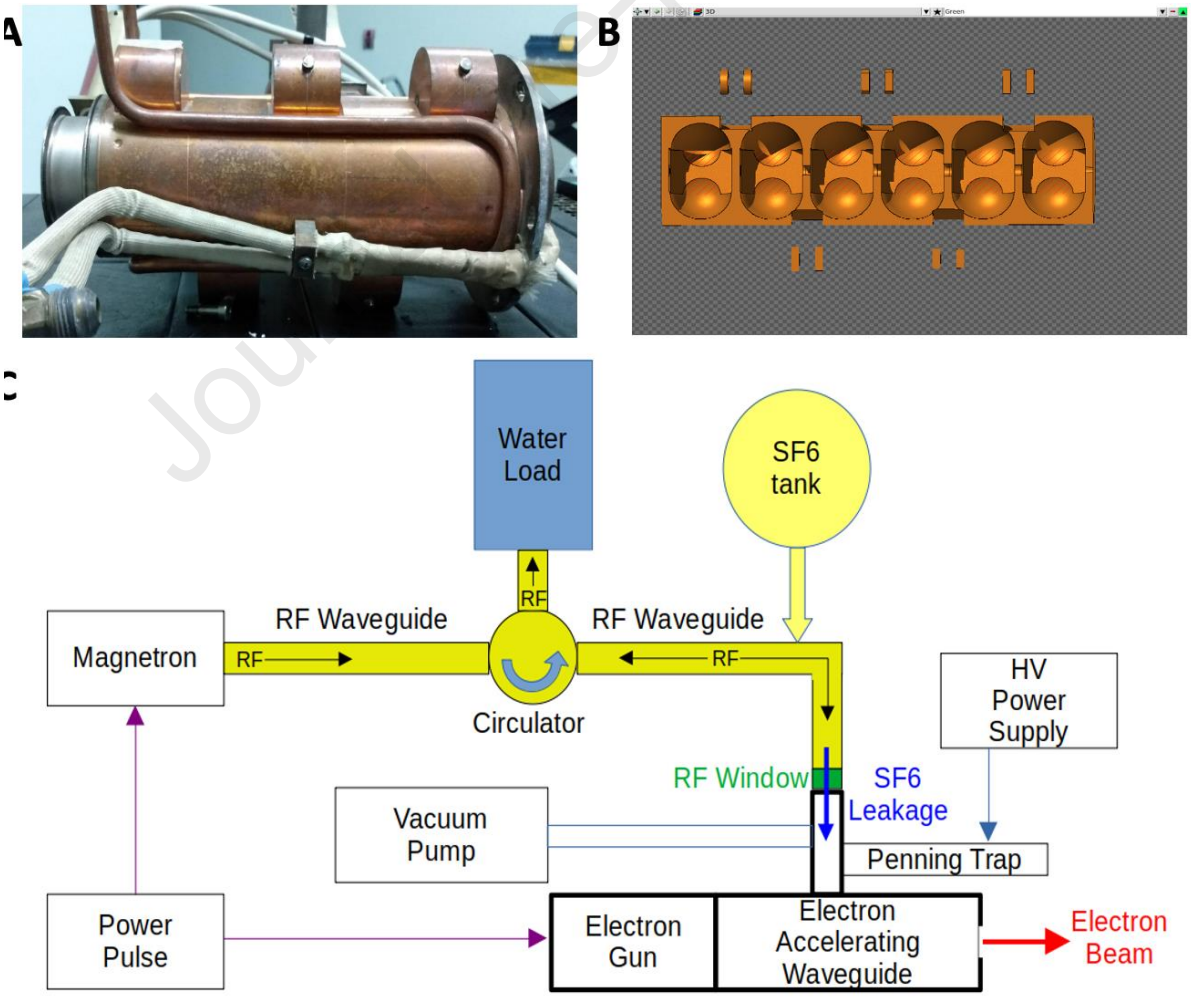

Figure 2: Accelerating waveguide of the VARIAN 6/100 linac: picture of an actual waveguide (**A**) and 3-D view of the corresponding MC simulation model for the vacuum case (**B**) along with a simplified block diagram sketching the basic operation of a typical linac waveguide (**C**). Waveguide cavities are fulfilled with gas, air or $SF_6$, when considering the presence of matter inside. Electrons are initiated in the first dynode (left side) and the electric field defined along the longitudinal ($z$) axis is responsible for the acceleration.

FLUKA simulations have been performed for the different setups running 5 independent cycles of $10^8$ primary particles each one. The simulated waveguide central axial region has been virtually divided into equivalent regions; each one 1 cm thick. The fluence of primary particles (injected electrons), (total) electrons, and photons has been recorded at the interfaces between these virtual regions, thus obtaining particles' spectra 1 cm aside along the waveguide longitudinal axis. In addition, the absorbed energy and particles' intensity along the entire cavity have been assessed. The *EMFCUT* card has been used in the FLUKA inputs to set the transport cut-off and absorption energy values for charged particles and photons, which have been set to 5 keV in all cases.

## Electric field and thermodynamic conditions in the waveguide

Considering a point particle with charge $q$ in presence of an electric field $\vec{E}$, the kinetic energy variation ($\Delta T$) due to the work ($W$) done by the field can be obtained from expression (1):

$$\Delta T = W = \int q\,\vec{E}\cdot d\vec{s} \qquad (1)$$

where $C$ denotes de track followed by the charged particle along the $\vec{s}$ traveling path. Then, for the stationary (steady state) field approximation and considering a piecewise constant longitudinal electric field, the kinetic energy variation at different waveguide positions for electrons longitudinally traveling the waveguide as accelerated by the electric field can be straightforwardly assessed by means of expression (2):

$$\Delta T(z) = \sum_j \quad q_e \left|\vec{E}\right|_j z_j = q_e \left[\left|\vec{E}\right|_1 z_1 + \ldots + \left|\vec{E}\right|_N z_N\right] \qquad (2)$$

where $q_e$ is the elemental electron charge ($1.602\ 10^{-19}$ C, approximately) and $z$ is the longitudinal coordinate that ranges between 0 (injection point) and $L$, the waveguide length, *i.e.*, ~30 cm. The total length $L$ has been subdivided into $N$ steps according to the $N$ intervals of the piecewise constant approximation of the electric field. Thereby, if $\langle E\rangle$ is the mean value of the electric field $\vec{E}$ -a physical and thus a differentiable operator- in the range $[0, L]$, $\Delta T$ can be obtained in terms of the Riemann framework. In this context, $\langle E\rangle$ represents the uniform field intensity capable of producing the same effective kinetic energy variation, *i.e.*: $\langle E\rangle \sim$ 6 MeV/(0.3 m $q_e$) = 20 MV/m for the 6 MV 6/100 VARIAN linac waveguide, assuming electrons are injected almost at rest. Accordingly, a 20 MV/m uniform longitudinal electric field should produce a 6 MeV electron beam reaching the target or emerging the waveguide if the target is removed.

Technically, the electric field has been defined in the FLUKA simulations through an external routine specially adapted for the aims of this work. Based on the description for the

dependence on the longitudinal coordinate of the field given by Whelan et.al. (Whelan et.al., 2016), the Fortran 77 FLUKA subroutine *elefld.f* has been suitably adjusted and carefully modified to externally incorporate the electric field properties. This allows any user-defined electric field distribution, particularly the piecewise constant approximation provided by Whelan. Due to the periodicity among dynodes, knowing the electric field inside one of them provides the whole required information, as depicted by Figure 3. It is worth remarking that the mean value of the electric field intensity approaches $\langle E \rangle \sim 20$ MV/m, as expected provided that electrons entering the cavity achieve a kinetic energy of 6 MeV at the end of their journey through the waveguide.

For guaranteeing a proper acceleration and functioning of the proposed electric field, the case of a 20 MV/m uniform one has been studied at a first instance.

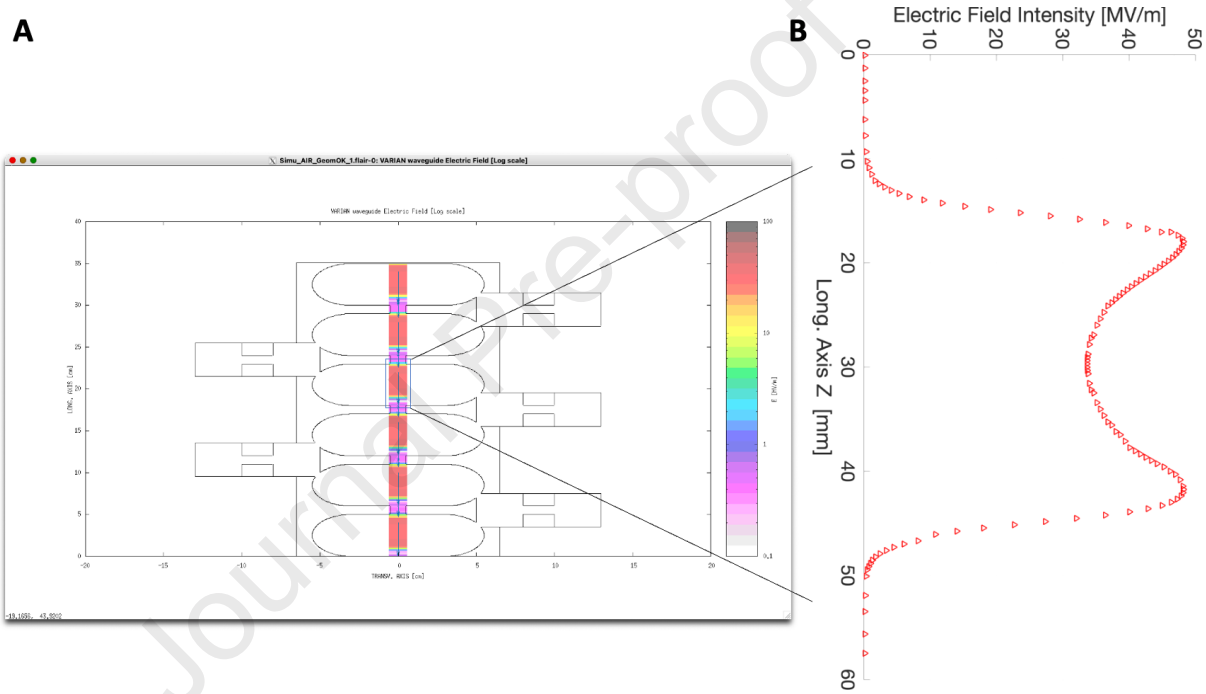


Figure 3: Map of the electric field intensity inside the linac waveguide (**A**) along with the corresponding dependence upon the longitudinal coordinate axis for one dynode (**B**).

In accordance with VARIAN 6/100 linac waveguide parameters, the kinetic energy of the injected electrons has been set to tenths of keV (VARIAN, 1981). Consequently, primary particles correspond to electrons with an initial kinetic energy close to rest from one end of the cavity and start to travel through the main axis of it to the other end point, under the influence of the electric field.

Additionally, the presence of air or SF6 has been introduced inside the waveguide. For the former, the material definition and properties provided by the code distribution package database have been used. Meanwhile, for the sulfur hexafluoride it has been necessary to realize its user definition. For that end, the Bragg-Kleeman additivity rule has been used with the aim of estimating the compound properties (Ulmer & Matsinos, 2010; Mustapha et.al., 2017; Valente et al., 2018). Table 1 summarizes the parameters used for designing the material, by means of a specific card present in the simulation input file.

| | N [w/w] | O [w/w] | S [w/w] | F [w/w] | Ar [w/w] | Mass density [g cm$^{-3}$] | Mean excitation energy [eV] |
|---|---|---|---|---|---|---|---|
| **SF6** | - | - | 0.7805 | 0.2195 | - | 0.00617 | 127.4 |
| **Dry air** | 0.755 | 0.232 | - | - | 0.013 | 0.00120479 | 85.7 |

Table 1: Parameters used for dry air (sea level) and $SF_6$ compounds (under 1 atm pressure conditions) according to the NIST database and the Bragg-Kleeman rule.

As noticed, the gas pressure plays a key role in the effects on the accelerating electron fluence. Attempting to point out its influence, different thermodynamics conditions have been studied representing variations from 1 atm to $10^{-5}$ atm. By virtue of the ideal gas law (Reichl, 2016; Callen, 1981), volumetric density of scattering centers depends linearly on the pressure. Subsequently, working within the framework of non-structured materials, variations in mass density have been used to represent the presence of gasses having different pressures, but being in equilibrium with the temperature of the external normal thermodynamic conditions. The different considered simulation setups are summarized in Table 2.

| Setup ID | Waveguide interior | Electric Field [MV/m] | Pressure [atm] |
|---|---|---|---|
| Vac-Unif | vacuum | (0, 0, -20) | - |
| Vac-Non Unif | vacuum | piecewise $\vec{E}(z)$ in Fig. 3 | - |
| Air-1 | air | piecewise $\vec{E}(z)$ in Fig. 3 | 1 |
| Air-$10^{-2}$ | air | piecewise $\vec{E}(z)$ in Fig. 3 | $10^{-2}$ |
| Air-$10^{-5}$ | air | piecewise $\vec{E}(z)$ in Fig. 3 | $10^{-5}$ |
| Air-$10^{-6}$ | air | piecewise $\vec{E}(z)$ in Fig. 3 | $10^{-6}$ |
| SF6-1 | SF6 | piecewise $\vec{E}(z)$ in Fig. 3 | 1 |
| SF6-$10^{-2}$ | SF6 | piecewise $\vec{E}(z)$ in Fig. 3 | $10^{-2}$ |
| SF6-$10^{-5}$ | SF6 | piecewise $\vec{E}(z)$ in Fig. 3 | $10^{-5}$ |
| SF6-$10^{-7}$ | SF6 | piecewise $\vec{E}(z)$ in Fig. 3 | $10^{-7}$ |

Table 2: Simulation setups.

The *STEPSIZE* FLUKA card has been used to limit the absolute length of the particle step during its tracking, aiming to ensure that steps be smaller than the dimensions of the current region and of those surrounding it. Simulations have been carried out on Intel core i7 3.2 GHz processors requiring, approximately, 60 hours per setup obtaining overall statistical uncertainties less than 3 %.

## Results and discussions

The principal measured magnitudes in the cavity of the waveguide are reported in Figure 4. It shows spatial distribution of absorbed energy along with the primary particle, total electrons, and photon fluence, for the case of SF6 at $10^{-2}$ atm of pressure.

On the other hand, electron energy output spectra in vacuum can be appreciated in Figure 5. The left figure reports the obtained results for the case of the uniform electric field along the waveguide, meanwhile the right one shows the case of the spatially dependent electric field described in Figure 3. As expected, since the intensity of the constant field ($\langle E \rangle$) corresponds, approximately, to the expectation value of the variable one ($\frac{\int \vec{E} \cdot d\vec{z}}{\int d\vec{z}}$), it can be seen how in both cases the reported electrons' final energy is almost the same. Since the functional dependence with the longitudinal coordinate is not the same for both cases, the acceleration process is naturally different. However, it is worth remarking that the final results are quite the same.

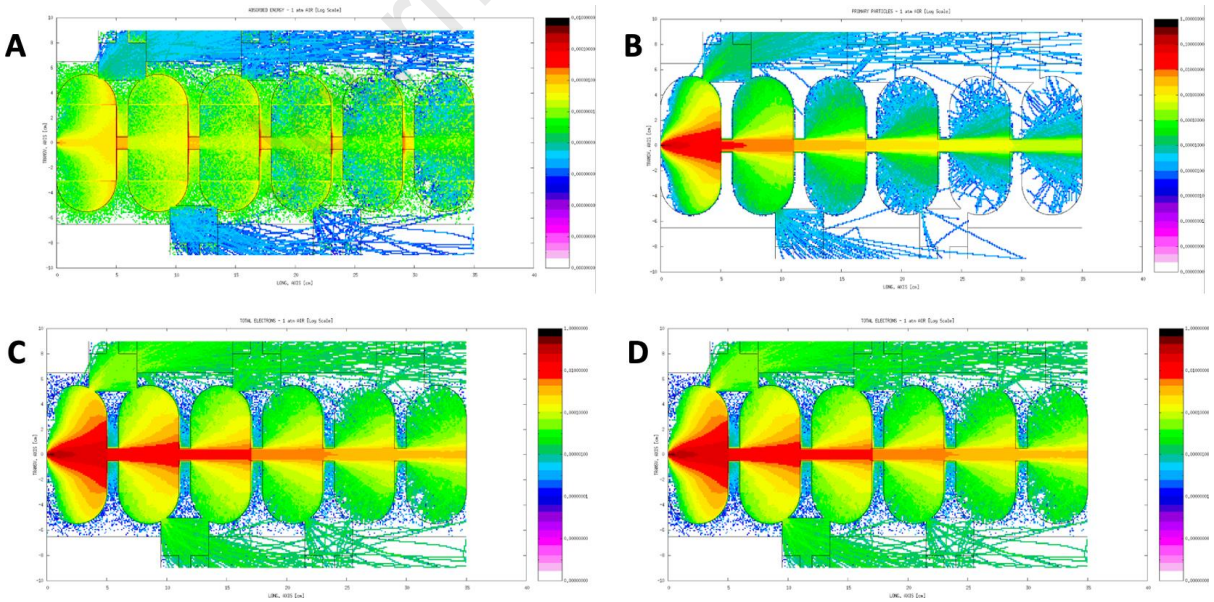


Figure 4: Absorbed energy (**A**) along with fluence of primary particles (**B**), total electrons (**C**) and photons (**D**), as a function of the longitudinal coordinate of the waveguide for the SF6 at $10^{-2}$ atm case, as depicted by the *FLAIR* interface. Results are shown using a logarithmic scale color bar and over imposed to the waveguide geometry (black lines behind the plots). Colorbars' scales are adjusted to their own figure visualization optimization.

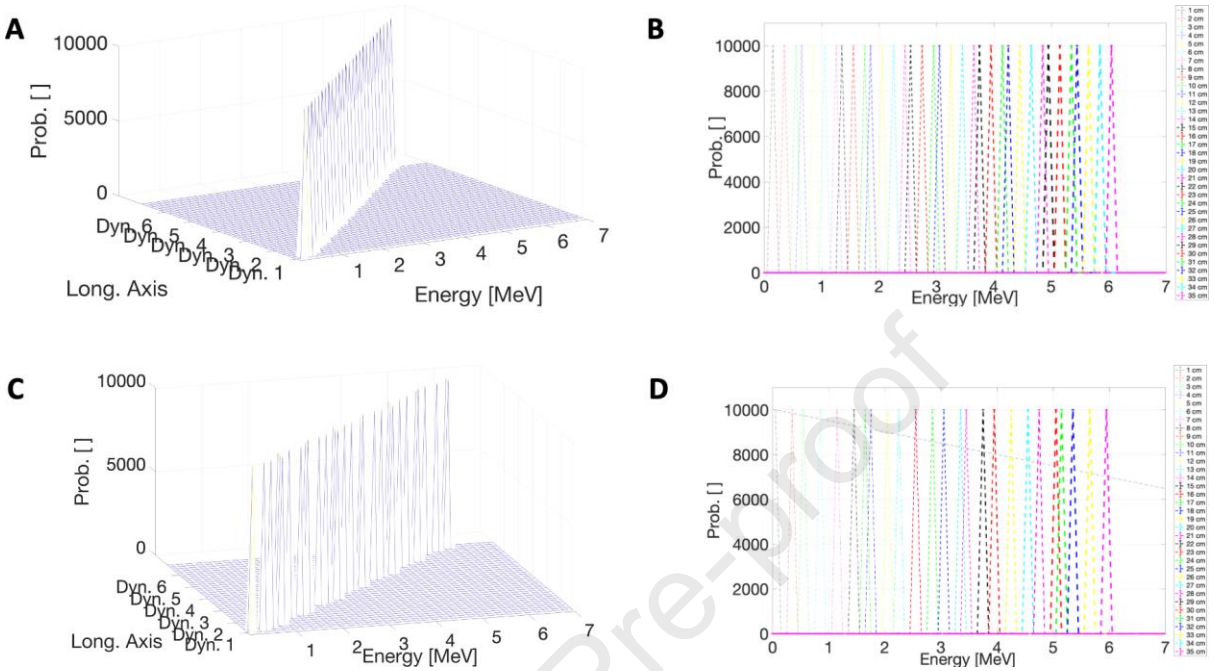


Figure 5: Electron energy spectra in vacuum for uniform (**A** and **B** on the top) and spatially dependent (**C** and **D** on the bottom) electric field as a function of the longitudinal position while primary electrons travel across the six dynodes. Legends and colors in graphs **B** and **D** denote spectra at different travel distances inside the waveguide, from the injection point to the exit window, each 1 cm.

Aimed at pointing out the pressure effects, Figure 6 reports the spectral distribution of the electron kinetic energy as a function of pressure of the gas inside the waveguide, for electrons crossing from the first to the second dynode. For both materials, air and SF6, the kinetic energy decreases as the pressure increases. This behavior is expected due to the correlation proposed between the pressure and the volumetric density of scattering centers. An increase in the former leads to a larger number of interactions of the accelerated electrons with the scattering medium, decreasing the maximum kinetic energy that they can reach. For the same reason, when comparing the results for the air (left) and SF6 (right), due to both mass density and cross section differences, the electron fluence spectra are differently affected, producing lower effect in the air for the same pressure conditions.

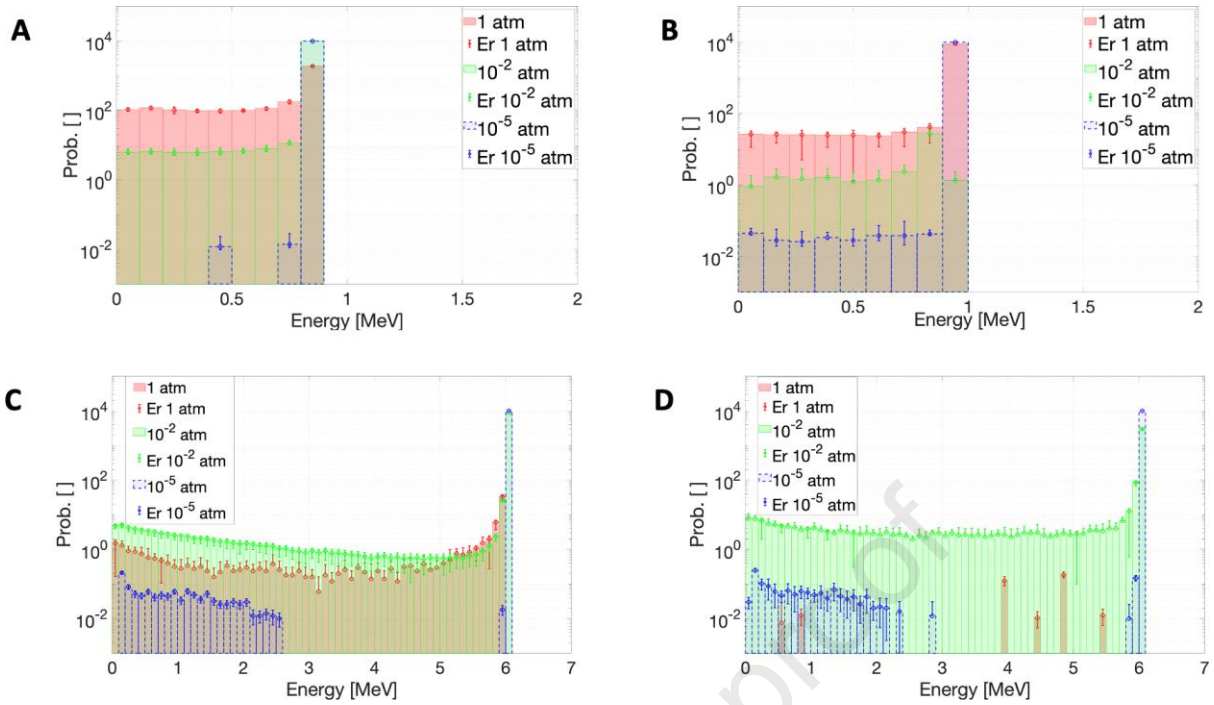


Figure 6: Kinetic energy spectral distribution of the electron fluence for air (**A** and **C**) and SF6 (**B** and **D**) at different pressures using the spatially dependent electric field: electrons crossing from the first to the second dynode (**A** and **B**) and reaching the waveguide exit window, *i.e.* leaving the sixth dynode (**C** and **D**).

It's worth mentioning that for the level of statistical representation used, the air behavior at $\sim 10^{-6}$ atm resembles that of a vacuum in the asymptotic limit. Similar trend is observed at $\sim 10^{-7}$ atm for the SF6, due to its higher mass density in comparison. Regarding the differences between uniform and spatially dependent steady-state electric fields, it should be noticed that the kinetic energy of primary electrons reaching the waveguide exit window must be assessed in accordance with the expression (2): $\Delta T(L) = \sum_j q_e \vec{E}_j z_j \approx \langle E \rangle L = 6$ MeV, which holds for the vacuum, but does not apply when matter is present in the system.

In this regard, some key issues should be stated when considering gas inside the waveguide: firstly, interactions with gas molecules modify the primary electrons' kinetic energy creating, eventually, secondary particles. Secondly, if energy losses due to interactions are high enough, primary electrons injected with a few tens of keV might be completely stopped if the electric field intensity is not high enough in the first part of the injection dynode. Therefore, this noticeable difference between the uniform and the spatially dependent electric fields (refer to Figure 3) may produce significant performance differences according to the electric field properties, mainly when considering higher interaction probabilities, as happens at high pressure levels.

Comparing the emerging electron energy (output) spectra for the case of vacuum, which represents the ideal situation, with cases in presence of gasses, it can be noticed in first place the obvious absence of scattering radiation. On the other hand, when the waveguide operates without gas filtration, the energy of primary electron bunches varies according to the distance traveled in the guide following exclusively the electrodynamics laws. These results have a great

utility for carrying out auto-consistency and contrast tests with analytical models. Moreover, differences between uniform and spatially dependent steady-state electric fields, as reported in Figure 5, can be clearly depicted providing results in complete agreement with electrodynamics (refer to the linear relationship shown top right in Figure 5).

Additionally, Figure 7 summarizes the consistent trend for the primary (injected) electrons found for the output spectra at a fixed pressure condition ($10^{-2}$ atm) along with the vacuum case considering uniform and spatially dependent steady-state electric field conditions. As appreciated, collisions due to the presence of infiltrated gas affect the kinematic properties of the injected electrons, regardless of the electric field properties. Thus, the amount of primary and total electrons that reach the exit window of the acceleration waveguide as well as their kinetic energy and propagation direction, can be significantly affected by any eventual gas infiltration, as represented by the tails at the left of the nominal exit energy, which should attain ideally 6.0 MeV. It is worth mentioning that the value for the uniform electric field ($\langle E \rangle$) has been assigned with the aim of obtaining 6.0 MeV electrons at the waveguide exit window, while the spatially dependent electric field intensities have been assessed as good as possible from (Whelan et.al., 2016). Therefore, minor differences, as shown in Figure 7, may be attributable to this issue.

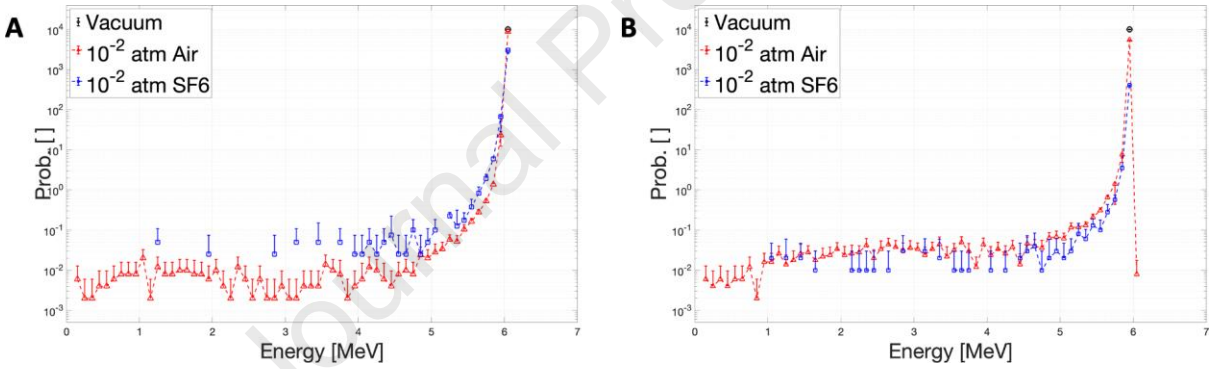


Figure 7: Energy spectrum of primary electrons reaching the waveguide exit window for vacuum and $10^{-2}$ atm gasses considering uniform (**A**) and spatially dependent steady-state (**B**) electric fields.

According to the obtained results, interactions with the unfiltered gas reduce the primary particles' kinetic energy. Thereby, attention should be called to the corresponding secondary particles' production because of such interactions. Secondary charged particles, mainly electrons, have been presented and discussed in Figures 4, 5, and 6; whereas Figure 8 reports on the corresponding photon fluence spectra. As expected, the total amount of photons that is correlated with the area below the curve in Figure 8 increases as the interaction probability increases. Thus, for the studied configuration more photons reach the exit window if the pressure grows, or the cross section increases.

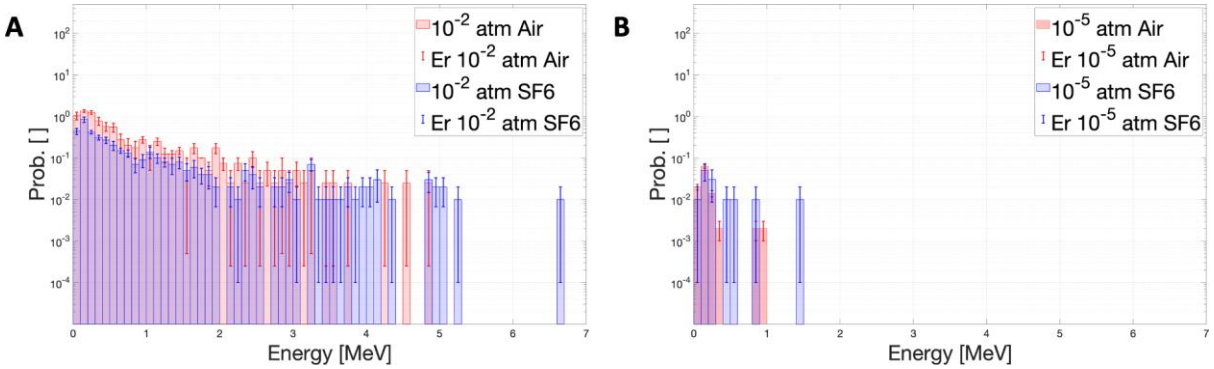


Figure 8: Spectrum of photons reaching the waveguide exit window for gasses at $10^{-2}$ (**A**) and $10^{-5}$ (**B**) atm.

## Conclusions

The present study shows qualitatively and quantitatively the effects on the electron bunches injected into the linac VARIAN 6/100 waveguide, due to the presence of gas inside the acceleration cavity.

Although the FLUKA simulation code is widely applied, it is worth remarking the level of detail and the degree of adaptation and application to the specific waveguide problem that is part of the CONVERAY project at the Center for Physics and Engineering for Health (CFIS) - Universidad de la Frontera - Chile. Moreover, both uniform and spatially dependent realistic steady-state electric fields have been successfully incorporated into the simulation model, simultaneously with the presence of gas inside the cavity. Achieved information confirms that the air or SF6 affects the transport and collision properties of the electrons injected into the waveguide. The degradation of their energy spectrum strongly depends upon the kind of gas that could be leaked and the thermodynamic conditions, mainly the pressure.

The developed methodologies and tools could also respond and be applied in other circumstances where the specific needs of the research objective require modifications to the accelerator equipment, compromising the vacuum system of the device, regardless of the CONVERAY project. Access to an affordable tool to assess electron spectral degradation as a function of gas type and pressure is critical to determining the required vacuum levels for specific waveguide applications, as it provides a better understanding and robustness of the problem situation, as well as offers an answer to a problem which would be complex to solve if not numerically studied.

In practical terms, the obtained results presents valuable information for the experimental situations in which there is suspected the possibility of SF6 leakage or loss of hermetic sealing in the waveguide at the CONVERAY project (Figueroa & Valente, 2015). The maximum values of kinetic energy achieved by the electrons have been obtained as a function of the type of gas, considering pressures from 1 atm to $10^{-5}$ atm. It should be noted that within the statistical level used in the numerical study, at around $10^{-6}$ atm, air behaves similarly to a vacuum statistically, while SF6 follows a similar trend at approximately $10^{-7}$ atm due to its higher density

## Acknowledges

Authors specially thanks the Center for Physics and Health Engineering, CFIS, from Universidad de la Frontera, and project CONVERAY - FONDEF IT19I0108, for the technical information provided. A.G. thanks to CONICET Argentina for her PhD. fellowship as well as to the medical physics MSc. program at UFRO for the partially supporting the research stage at University of La Frontera. This work used computational resources from CCAD – Universidad Nacional de Córdoba (https://ccad.unc.edu.ar/), which are part of SNCAD – MinCyT, República Argentina.

Author Contributions: Conceptualization: M.V., R.F.; methodology: M.V., A.G., F.M., R.F.; J.G.; software: M.V., F.M., A.G., J.G.; formal analysis: A.G., M.V., R.F.; investigation: M.V., A.G., F.M., R.F., J.G., J.L., F.L.; resources: M.V., R.F.; data curation: A.G., F.M., J.G., J.L., F.L.; writing-original draft preparation: A.G., M.V., F.M.; writing-review and editing, M.V., A.G., F.M., J.G., R.F.; visualization: A.G., F.M.; supervision: M.V., R.F.; project administration: R.F., M.V.; funding acquisition: R.F., M.V. All authors have read and agreed to the published version of the manuscript.

## References

**(Aubin et.al., 2010)** Aubin J.S., Steciw S., Kirkby C., Fallone B.G. (2010) *An integrated 6 MV linear accelerator model from electron gun to dose in a water tank*. Med. Phys, 37(5), American Association of Physicists in Medicine. https://doi.org/10.1118/1.3397455

**(Aubin et.al., 2015)** Aubin J., Keyvanloo A., Vassiliev O., Fallone B.G. (2015) *A deterministic solution of the first order linear Boltzmann transport equation in the presence of external magnetic fields*. Med. Phys. 42, 780-793. https://doi.org/10.1118/1.4905041

**(Baillie, 2016)** Baillie D.M.J (2016) *Design and simulation of a short, 10 MV, variable energy linear accelerator for use in linac-MR systems*. Department of Oncology, University of Alberta

**(Battistoni et.al., 2016)** Battistoni G., Bauer J., Boehlen T., Chin F. C. M. P., Augusto R. D. S., Ferrari A., Kozlowska P. G. O. W., Magro G., Mairani A., Parodi K., Sala P. R., Schoofs P., Tessonnier T., Vlachoudis V. (2016) *The FLUKA Code: An Accurate Simulation Tool for Particle Therapy*. Frontiers in Oncology 6 , 116. https://doi.org/10.3389/fonc.2016.00116

**(Battistoni et al., 2011)** Battistoni, G., Broggi, F.,Brugger, M., Campanella, M., Carboni, M., Empl, A., Fassò, A., Gadioli, E., Cerutti, F., Ferrari, A., Ferrari, A., Lantz, M., Mairani, A., Margiotta, M, Morone, C., Muraro, S., Parodi, K., Patera, V., Pelliccioni, M., Pinsky, L., Zapp, N. (2011) *Applications of FLUKA Monte Carlo code for nuclear and accelerator physics.* Nucl. Instrum. Meth. B, 269(24), 2850-2856. https://doi.org/10.1016/j.nimb.2011.04.028

**(Berger, 1963)** Berger M.J. (1963) *Monte Carlo calculation of the penetration and diffusion of fast charged particles*. Methods in Computational Physics. 1, 135-215

**(Bielajew & Boulevard, 2000)** Bielajew A.F., Boulevard B. (2000) *Fundamentals of the Monte Carlo method for neutral and charged particle transport*.

**(Bohlen et.al., 2014)** Bohlen T., Cerutti F., Chin M., Fasso A., Ferrari A., Ortega P., Mairani A., Sala P., Smirnov G., Vlachoudis V. (2014) *The FLUKA Code: Developments and Challenges for High Energy and Medical Applications*. Nuclear Data Sheets 120, 211-214. https://doi.org/10.1016/j.nds.2014.07.049

**(Callen, 1981)** Callen H.B. (1981) *Thermodynamics*. Alfa Centauro

**(Ehret, 2016)** Ehret M. (2016) *TNSA-Proton Beam Guidance with Strong Magnetic Fields Generated by Coil Targets*. https://dor.org/10.13140/RG.2.1.3855.7847

**(European Standards, 2021)** European Standards (2021) European Document EN 62271-1:2017, High-voltage switchgear and controlgear - Part1: Common specifications for alternating current switchgear and controlgear

**(Ferrari et.al., 2021)** Ferrari A., Sala P.R., Fass`o A., Ranft J. (2021) *Fluka: a multi-particle transport code*. CERN

**(Figueroa & Valente, 2015)** Figueroa R.G., Valente M. (2015) *Physical characterization of single convergent beam device for teletherapy: Theoretical and Monte Carlo approach.* Phys. Med. Biol., 60, 7191-7206. https://doi.org/10.1088/0031-9155/60/18/7191

**(Figueroa et.al., 2015)** Figueroa R.G., Santibáñez M., Malano, F., Valente M. (2015) *Optimal configuration for detection of gold nanoparticles in tumors using Kβ X-ray fluorescence line*. Rad. Phys. Chem., *117*, 198-202, https://doi.org/10.1016/j.radphyschem.2015.08.017

**(Figueroa et.al., 2016)** Figueroa R.G., Santibáñez M., Valente M. (2016) *Dosimetric and bremsstrahlung performance of a single convergent beam for teletherapy device*. Eur. Jour. Med. Phys., *32*, 1489-1494, https://doi.org/10.1016/j.ejmp.2016.10.003

**(Figueroa & Valente, US20140112451A1)** Figueroa R.G., Valente M., Convergent photon and electron beam generator device. U.S. patent US20140112451A1.

**(Gayol et.al., 2022)** Gayol, A., Vedelago, J., Valente, M. (2022). *MRI-LINAC dosimetry approach by Monte Carlo codes coupling charged particle radiation transport with strong magnetic fields*. Rad. Phys. Chem., 200. https://doi.org/10.1016/j.radphyschem.2022.110171

**(Glushkov et.al., 2014)** Glushkov D.A., Khalyasmaa A.I., Dmitriev S.A., Kokin S.E. (2014) *Electrical Strength Analysis of SF6 Gas Circuit Breaker Element*. AASRI Procedia, 7, 57-61. https://doi.org/10.1016/j.aasri.2014.05.029

**(Goller, 2008)** Goller S. (2008) *Investigation of high power limitation of waveguide elements at FLASH*. Institut für Experimentalphysik, Universität Hamburg

**(Gündem & Dirican, 2021)** Gündem E., Dirican B. (2021) *Analysis of characteristics and validation of 6 MV photon beam produced by Elekta Synergy linear accelerator using EGSnrc Monte Carlo code*. Radiation Physics and Chemistry, 184. https://doi.org/10.1016/j.radphyschem.2021.109491

**(Jackson, 1999)** Jackson J.D. (1999) *Classical electrodynamics*. John Wiley & Sons, INC

**(Karzmark & Morton, 1989)** Karzmark C.J., Morton R.J. (1989) *A primer on theory and operation of linear accelerators in radiation therapy*. Medical Physics Publishing Corporation

**(Khan, 2003)** Khan F.M. (2003) *The physics of radiation therapy*. LIPPINCOTT WILLIAMS & WILKINS

**(Kozłowska et.al., 2019)** Kozłowska, W.D., Böhlen, T.T., Cuccagna, C., Ferrari, A., Fracchiolla, F.. Mafro, G., Mairani, A., Schwarz, M., Vlachoudis, V., Georg, D. (2019) *FLUKA particle therapy tool for Monte Carlo independent calculation of scanned proton and carbon ion beam therapy*. Phys. Med. Biol., 64(7). doi: 10.1088/1361-6560/ab02c

**(Malano et.al., 2019)** Malano, F., Mattea, F., Geser, F.A., Pérez, P., Barraco, D., Santibáñez, M., Figueroa, R., Valente, M. (2019) *Assessment of FLUKA, PENELOPE and MCNP6 Monte Carlo codes for estimating gold fluorescence applied to the detection of gold-infused tumoral volumes*. Appl. Rad.Isot., 151, 280-88. https://doi.org/10.1016/j.apradiso.2019.06.017

**(Mohammed et.al., 2018)** Mohammed M., El Bardouni T., Chakir E., Boukhal H., Saeed M., Ahmed A. (2018) *Monte Carlo simulation of Varian Linac for 6MV photon beam with BEAMnrc code*. Radiation Physics and Chemistry, 144, 69-75, https://doi.org/10.1016/j.radphyschem.2017.11.017

**(Mustapha et.al., 2017)** Mustapha K., Harakat N., Khouaja A., Inchaouh J., Mesradi M.R., Chakir H., Kartouni A., Marouane A., Benjelloun M., Boudhaim S., Fiak M., Bouhssa M.L., Housni Z. (2017) *Method for range calculation based on empirical models of proton in liquid water: Validation study using Monte-Carlo method and ICRU data.* International Journal of Scientific & Engineering Research, 8, 728-735. https://dor.org/10.14299/ijser.2017.03.007

**(Pedersen, 1989)** Pedersen A. (1989) *On the electrical breakdown of gaseous dielectrics - an engineering approach*. IEEE Transactions on Electrical Insulation, 24(5), 721-739. https://doi.org/10.1109/14.42156

**(Podgorsak, 2005)** Podgorsak E.B. (2005) *Radiation oncology physics: A handbook for teachers and students*. INTERNATIONAL ATOMIC ENERGY AGENCY

**(Podgorsak, 2006)** Podgorsak E.B. (2006). *Radiation physics for medical physicists*. Springer

**(Reece et.al., 2001)** Reece C., Benesch J., Preble J. (2001) *Refining and maintaining the optimal performance of the CEBAF SRF systems.* PACS2001. Proceedings of the 2001 Particle Accelerator Conference (Cat. No.01CH37268), Chicago, IL, USA, 2001, pp. 1186-1188 vol.2. doi: 10.1109/PAC.2001.986622.

**(Reichl, 2016)** Reichl L.E. (2016) *A Modern Course in Statistical Physics*. WILEY-VCH Verlag GmbH & Co

**(Rodriguez Castillo et.al., 2020)** Rodriguez Castillo M.L., Brualla L., Sempau J. (2020) *Monte Carlo simulation of a Varian's TrueBeam linac as a Clinac 2100: A feasibility study*. Radiotherapy and Oncology, Volume 152, Supplement 1, https://doi.org/10.1016/S0167-8140(21)01411-0

**(Sickafus et.al., 2007)** Sickafus K., Kotomin E., and Uberuaga B. (2007) *Radiation Effects in Solids*. NATO Science Series.

**(Ulmer & Matsinos, 2010)** Ulmer W., Matsinos E. (2010) *Theoretical methods for the calculation of Bragg curves and 3D distributions of proton beams*. Eur. Phys. J. Spec. Top. 190, 1-81. https://doi.org/10.1140/epjst/e2010-01335-7

**(Valente et.al., 2007)** Valente M., Aon, E., Brunetto, M., Castellano, G., Gallivanone, F., Gambarini, G. (2015) *Gel dosimetry measurements and Monte Carlo modeling for external radiotherapy photon beams. Comparison with a treatment planning system dose distribution*. Nucl. Instrum. Meth. A 580, 497-501. https://doi.org/10.1016/j.nima.2007.05.243

**(Valente et.al., 2018)** Valente M., Vedelago, J., Chacón, D., Mattea, F., Velásquez, J., Pérez, P. (2018) *Water-equivalence of gel dosimeters for radiology medical imaging*. Appl. Rad. Isot. 141, 193-198. https://doi.org/10.1016/j.apradiso.2018.03.005

**(Vedelago et.al., 2018)** Vedelago, J. Mattea, F., Valente M. (2018) *Integration of Fricke gel dosimetry with Ag nanoparticles for experimental dose enhancement determination in theranostics*. Appl. Rad. Isot. 141, 182-186. https://doi.org/10.1016/j.apradiso.2018.02.028

**(VARIAN, 1981)** Varian associates Inc. (1981) *Clinac 6/100 - 4/100 Maintenance Manual*
**(Wangler, 1989)** Wangler T. (1989) *Principles of RF linear accelerators*. John Wiley & Sons, INC
**(Whelan et.al., 2016)** Whelan B., Gierman S., Holloway L., Schmerge J., Keall P., Fahrig R. (2016) *A novel electron accelerator for MRI-Linac radiotherapy*. Medical Physics, 43(3), American Association of Physicists in Medicine. http://dx.doi.org/10.1118/1.4941309
**(Whittum, 1998)** Whittum D.H. (1998) *Introduction to Electrodynamics for Microwave Linear Accelerators*. Joint CERN-US-Japan Accelerator School: Course on Frontiers of Accelerator Technology: RF Engineering for Particle Accelerators, 1-135.
**(Wisnivesky et.al., 1997)** Wisnivesky D., Rafael F.S., Bagnato O.R., Picoli R.A., Lira A.C., Silva A.R., Pardine C. (1997) *Upgrading of the LNLS injection system*. Proceedings of the 1997 Particle Accelerator Conference (Cat. No.97CH36167), 1209-1211 vol.1. doi: 10.1109/PAC.1997.749978.
**(Wroe et.al., 2019)** Wroe L.M., Asogwa O.C., Aruah S.C., Grover S., Makufa R., Fitz-Gibbon M., Sheehy S.L. (2019) *Comparative Analysis of Radiotherapy Linear Accelerator Downtime and Failure Modes in the UK, Nigeria and Botswana*. Clinical Oncology, 32, e111-e118. https://doi.org/10.1016/j.clon.2019.10.010
**(Yaqub et.al., 2021)** Yaqub K., Akbar S., Javeed S., Siddique F., Rahman A., Nisar N., Khalid M.F., Saqib N.U., Khan M.A. (2021) *Design, simulation and implementation of an efficient vacuum system and gas load calculations for a 6 MeV industrial LINAC*. Vacuum, 187. https://doi.org/10.1016/j.vacuum.2021.110151
**(Zangwill, 2012)** Zangwill A. (2012) *Modern electrodynamics*. Cambridge University Press

# HIGHLIGHTS

- Effects of gas in linac waveguide are characterized by adapting the FLUKA Monte Carlo main code.
- Electric field coupling is attained to model injected electrons in the VARIAN 6/100 linac waveguide.
- Differences between uniform and spatially dependent electric fields are studied.
- Longitudinal fluence of primary, electrons and photons are reported considering different gas thermodynamic conditions.
- Agreement with electromagnetic laws is achieved for vacuum.

**Declaration of interests**

☒ The authors declare that they have no known competing financial interests or personal relationships that could have appeared to influence the work reported in this paper.

☐The authors declare the following financial interests/personal relationships which may be considered as potential competing interests: